Acta Societatis Botanicorum Poloniae

DOI: 10.5586/asbp.3602

Publication history
Received: 2018-06-29
Accepted: 2018-11-26
Published: 2018-12-31

Handling editor
Bronisław Wojtuń, Faculty of Biological Sciences, University of Wrocław, Poland

Funding
The work was supported by projects of the Ministry of Education, Youth and Sports LM2015078 – CzechPolar2 and ECOPOLARIS – CZ.02.1.01/0.0/0.0/16_013/0001708.

Competing interests
No competing interests have been declared.

Citation
Kvíderová J. Internal structure and photosynthetic performance of *Nostoc* sp. colonies in the high Arctic. Acta Soc Bot Pol. 2018;87(4):3602. https://doi.org/10.5586/asbp.3602

ORIGINAL RESEARCH PAPER

Internal structure and photosynthetic performance of *Nostoc* sp. colonies in the high Arctic

Jana Kvíderová*

Center for Polar Ecology, Faculty of Science, University of South Bohemia in České Budějovice, Na Zlaté stoce 3, 370 05 České Budějovice, Czech Republic

* Email: jana.kviderova@objektivem.net

Abstract

The physiological performance of *Nostoc* sp. colonies in the high Arctic was investigated based on their structure and function. To investigate the internal colony structure, a method based on vertical stacking of individual light microscopy images was tested under the conditions at a polar field station. The physiological state of sun-exposed and shaded surfaces of the colonies was assessed using variable chlorophyll fluorescence imaging under two distinct low- and high-light conditions. The 3D image of the internal structure of the colonies revealed a high number of cells in the central part of the colony. Two peaks of maximum cell density were observed, probably caused by two overlapping colony lobes or subcolonies. Light was the driving factor of photosynthetic activity, and the colony structure played a role in the rate of response to incoming light. Fluorescence imaging revealed heterogeneity of the photosynthetic activity in the colonies, with the maximum photosynthetic activity at the colony edge due to better access to nutrients. The differences between exposed and shaded surfaces were not as pronounced as was expected, either due to good photoacclimation to a broad range of light conditions, light distribution through translucent extracellular matrixes, or integration of fluorescence signals throughout the colonies. The slightly better photosynthetic performance under high light conditions may indicate photoacclimation of *Nostoc* sp. to a broad range of light conditions encountered in the field.

Keywords

Nostoc sp.; photosynthesis; 3D structure; light microscopy; Arctic; fluorescence imaging

Introduction

In the Polar regions, algae and cyanobacteria are important, if not the only (in cases of specific and very extreme environments), primary producers in hydro-terrestrial and terrestrial ecosystems [1–5]. To survive in harsh polar environments, algae and cyanobacteria developed various mechanisms of adaptation/acclimation [5–7]. The strategies for coping with a stressor can be divided into stress tolerance, i.e., adaptation or acclimation to the given stress factor(s), or stress avoidance, i.e., escape from stressful conditions and/or insulation from surroundings [8].

One of the stress avoidance mechanisms is formation of consortia in which the central part is protected by surface layers. The consortia may be formed by one species (i.e., colonies, which are sometimes even macroscopic [9,10]), by several species (for example microbial mats [11] or soil crusts [12,13]) or, in the most extreme cases, by strictly symbiotic microorganisms (lichens) [14,15]. The structure of the consortia is similar for all types and consists of filamentous and amorphous components [16–18]. Furthermore, the ratio of the consortium components may reflect the species-specific internal structure, e.g., in lichens, or may be influenced by the environment, e.g., the

dependence of the amount of amorphous extracellular matrix in *Nostoc* sp. colonies on water availability [19].

These consortia are usually located at or near air-liquid, air-solid, or liquid-solid interfaces [16–18]. The area covered by a consortium may range from several μm^2 to mm^2 in the case of initial stages of *Nostoc* sp. colonies [9,20] or lichen development [21], respectively. In some cases, the area covered by a consortium can reach several dozen or even several hundred km^2 in the case of microbial mats in permanently frozen Antarctic lakes [22] or marine benthos communities [23]. The thickness of consortia usually varies from the order of tenths of μm to tenths of cm [22,24–26]. Since the environmental conditions on exposed and shaded surfaces, and within the consortium are different, environmental gradients develop in consortia [27–29], and physiological responses should reflect the internal structure of the consortia. The exposed surface layers may be exposed to higher temperatures than those in touch with the substrate. The exposed surface layers are also subjected to higher irradiances. Finally, a nutrient/water availability gradient develops inside the consortia, as the exposed superficial layers are subjected to nutrient deficiency, and air-exposed surfaces are also exposed to water availability deficiency.

Based on microscopic evaluation, the macroscopic colonies of *Nostoc* sp. (Cyanobacteria) represent a typical one-species consortium. However, application of molecular taxonomical methods revealed associated bacteria in macroscopic *Nostoc* sp. colonies [30], and therefore such colonies should be considered as multispecies consortia. *Nostoc* sp. colonies are an important source of carbon and nitrogen in polar hydro-terrestrial and terrestrial ecosystems [4,5,31]. Therefore, detailed knowledge of the interplay between the internal structure and the physiological performance of *Nostoc* sp. colonies, and the environmental conditions surrounding such colonies is crucial for the development of reliable models of *Nostoc* sp. primary production in situ. In this study, method to study the internal 3D structure of *Nostoc* sp. colonies was adjusted for using a light microscope, as the conditions at field polar stations (which include logistical challenges related to transport, and electric power supply, etc.) do not allow for the use of confocal or motorized light microscopes. The variable chlorophyll fluorescence imaging approach [32,33] was applied to determine the differences in photosynthetic activity between exposed and shaded sides of *Nostoc* sp. colonies under two distinct light conditions, as the exposed surface should be photoacclimated to higher irradiances.

Material and methods

Experimental site

The *Nostoc* sp. colonies were collected randomly at a seepage near the Nostoc Field Station of the Czech Arctic Research Infrastructure "Josef Svoboda Station" (78°40′ 50.268″ N, 16°27′27.72″ E, 4 m a.s.l.). Colonies of similar size (~1 cm^2) were collected using tweezers and placed into a Petri dish. The Petri dish was immediately stored under dark conditions for dark adaptation for the fluorescence measurement. The original orientation of the exposed and shaded side of the colonies was maintained during sampling and transfer to laboratory at the station.

Internal structure

A series of 69 microscopic photo shots of one colony was taken using an Olympus BX-53 light microscope and a DP-72 digital camera (both Olympus, Japan) at 2-μm intervals at vertical axis. The shift in the vertical axis was performed manually. The microphotographs were processed using ProMicra 2.3 software (ProMicra, the Czech Republic). Further microphotograph processing, image analysis, and construction of the 3D structure was performed using ImageJ 1.54 software [34].

To obtain the vertical profile of the cell content, the percentage of coverage was used as a proxy. The individual color microphotographs were calibrated, converted to gray-scale images, and binarized. The coverage was calculated from binarized images

using ImageJ 1.54 software [34]. The binarized images were used for construction of the 3D structure. Mean and standard deviation were calculated for each 6-μm interval on the vertical axis.

Two different models were tested to fit the data using SigmaPlot 10.0 (Systat Software, USA). The one-modal model was based on a three-parameter Gaussian curve, according to the following equation (as defined by Systat Software, USA):

$$C = ae^{\left[-0.5\left(\frac{D-D_0}{b}\right)^2\right]}$$

where D is the depth, C is the coverage, a and b are the parameters, and D_0 is the depth where the maximum occurs.

The two-modal model was based on the sum of two three-parameter Gaussian curves, according to the following equation:

$$C = a_1 e^{\left[-0.5\left(\frac{D-D_1}{b_1}\right)^2\right]} + a_2 e^{\left[-0.5\left(\frac{D-D_2}{b_2}\right)^2\right]}$$

where D is the depth, C is the coverage, a_1, a_2, b_1, and b_2 are the parameters, and D_1 and D_2 are the depths where the maxima occur.

For 2D visualization of the mucilaginous sheaths and extracellular colonial mucilage, a drop of Indian ink was added to the microscopic specimen.

Photosynthetic activity

The photosynthetic activity of the exposed and shaded surfaces of five *Nostoc* sp. colonies was measured on sunny (high light conditions, ~800 μmol m^{-2} s^{-1}) and on cloudy (low light conditions, ~350 μmol m^{-2} s^{-1}) days using a FluorCam FC-700 fluorescence imaging camera (Photon Systems Instruments, the Czech Republic). The data were processed using FluorCam 7 software (Photon Systems Instruments).

Before the fluorescence measurement, the colonies were subjected to 15 minutes of dark adaptation. The quenching protocol was applied as follows: the initial dark period for maximum quantum yield determination lasted 5 s when the saturation pulse was applied and was followed by 10 s of dark relaxation. The following red actinic light period of irradiance of 95 μmol m^{-2} s^{-1} lasted 60 s, and the saturation pulses were applied at 25, 37, 50, 62, and 75 s after the measurement was started. The short period of actinic light was selected to prevent colony heating during prolonged periods of measurement. After the actinic light period, a dark relaxation period lasting 20 s with one saturation pulse at 85 s after the start of the measurement was added. The intensity of the red measurement pulses was set to a maximum of 3 μmol m^{-2} s^{-1} and the pulses lasted 20 μs. The intensity of the white saturation pulse was set to 2,100 μmol m^{-2} s^{-1}, and the saturation pulse lasted 800 ms.

The maximum quantum yield (F_V/F_M) was calculated according to the equation in Roháček et al. [35]:

$$F_V/F_M = \frac{F_M - F_0}{F_M}$$

where F_0 is the minimum fluorescence in the dark, and F_M is the maximum fluorescence after the saturation pulse in dark-adapted sample.

The effective quantum yield (Φ_{PSII}) was calculated according to the equation in Roháček et al. [35]:

$$\Phi_{PSII} = \frac{F'_M - F_S}{F'_M}$$

where F_S is the steady-state fluorescence in the light before the saturation pulse, and F_M' is the maximum fluorescence after the saturation pulse in the light-adapted sample.

The quantum yield in the dark relaxation period after the actinic light period (F_V''/F_M'') was calculated according to the equation in Roháček et al. [35]:

$$F''_V/F''_M = \frac{F''_M - F''_0}{F''_0}$$

where F_0'' is the minimum fluorescence before the saturation pulse, and F_M'' is the maximum fluorescence after the saturation pulse during dark relaxation after the actinic light period.

The nonphotochemical quenching (NPQ) was calculated according to the equation in Roháček et al. [35]:

$$NPQ = \frac{F_M - F'_M}{F'_M}$$

where F_M is the maximum fluorescence after the saturation pulse in the dark and F_M' is the maximum fluorescence after the saturation pulse in the light.

The photochemical quenching (q_P) was calculated according to equation in Roháček et al. [35]:

$$q_P = \frac{F'_M - F_S}{F'_M - F'_0}$$

where F_M' is the maximum fluorescence after the saturation pulse in the light, F_S is the steady-state fluorescence in the light before the saturation pulse, and F_0' is the minimum fluorescence immediately after the actinic light period.

The value of F_0' was calculated using the approximation of Oxborough and Baker [36]:

$$F'_0 = \frac{F_0}{\frac{F_M - F_0}{F_M} + \frac{F_0}{F'_M}}$$

where F_0 is the minimum fluorescence in the dark, F_M is the maximum fluorescence after the saturation pulse in the dark, and F_M' is the maximum fluorescence after the saturation pulse in the light.

Statistics

The statistical evaluations were performed using Statistica 13.2 software [37]. One-way analysis of variance (ANOVA) was used to test the dependence of the coverage on depth. Two-way ANOVA was used to test the effects of structure and light on photosynthetic activity and rate of change of the photosynthetic parameters. The results were considered significant at $p < 0.05$.

Results

Internal structure

One sequence of 69 microphotographs was found to be sufficient to create a 3D image of the *Nostoc* sp. colony. The 3D internal structure (Fig. 1) revealed heterogeneity of filament distribution in the internal structure of the *Nostoc* sp. colony.

The vertical profile revealed decreased cell coverage on the surface of the colony (one-way ANOVA; $n = 69$, $F = 30.73$, $p < 0.001$) (Fig. 2A,B). Two peaks of maximum coverage were found at depths of ca. 45 µm and 85 µm from the exposed surface; therefore, the two-modal model ($r^2 = 0.941$, $F = 57.13$, $p < 0.001$) (Fig. 2B) seemed to be better for description of the vertical profile than the one-modal one ($r^2 = 0.864$, $F = 66.89$, $p < 0.001$; Fig. 2A). It is likely that there were two overlapping lobes of the colony (Fig. 3).

Photosynthetic activity

The fluorescence imaging revealed heterogeneity of the photosynthetic activity inside of individual colonies as well as among the *Nostoc* sp. colonies. The maximum photosynthetic activity was usually observed at the edges of the colonies, and the minimum in their centers (Fig. 4A,B).

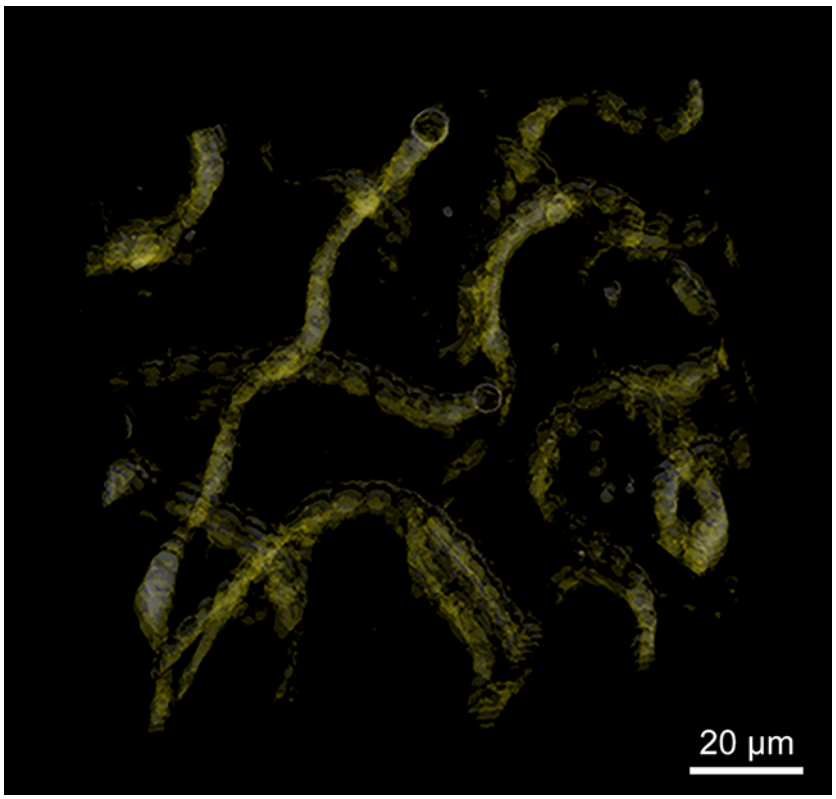

Fig. 1 The snapshot of the 3D internal structure projection of the *Nostoc* sp. colony, captured at the field station in Svalbard.

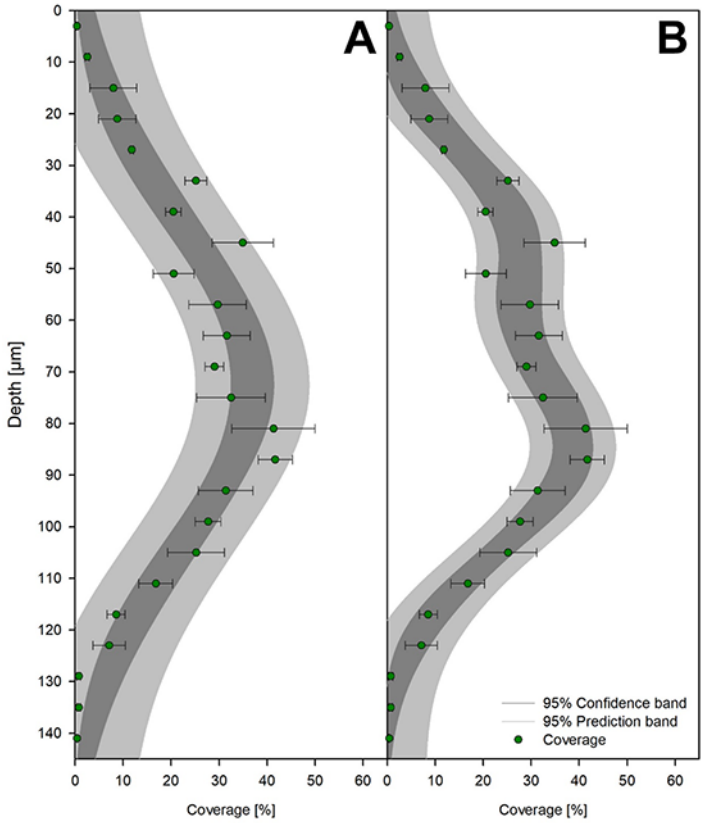

Fig. 2 Vertical profile of coverage (mean ±*SD*) of a *Nostoc* sp. colony. The means were calculated for 6 µm intervals, corresponding to cell diameters. (**A**) one-modal model; (**B**) two-modal model. 0 – exposed (upper) surface; maximum depth – shaded (lower) surface.

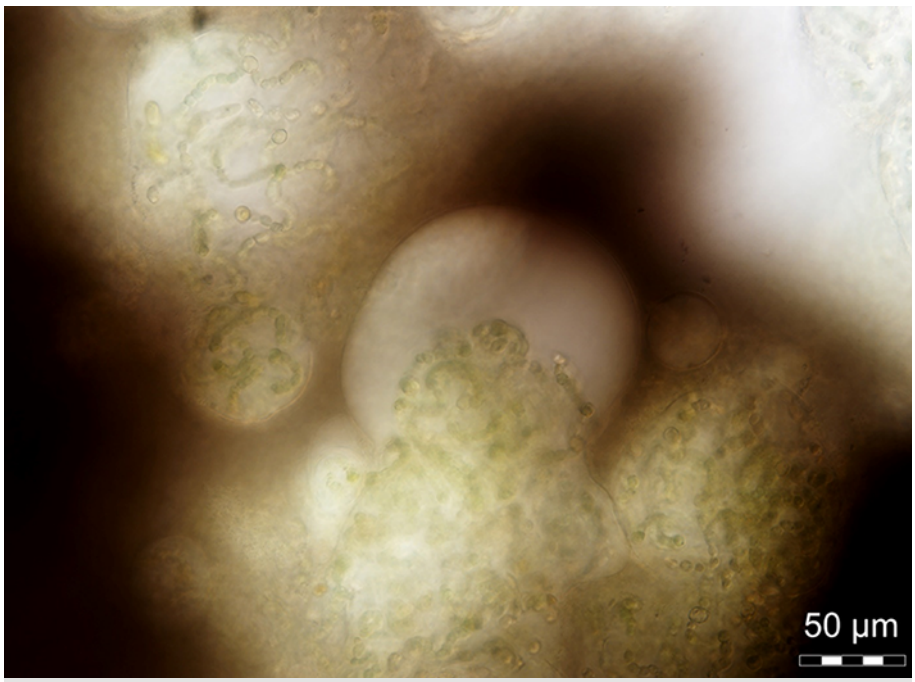

Fig. 3 Evidence of the overlapping lobes in the internal structure of a *Nostoc* sp. colony visualized using Indian ink staining.

Despite the heterogeneity, there was no statistically significant difference in F_0 (Fig. 4A). The light conditions played a more important role than the colony structure when considering their effects on fluorescence parameters F_V/F_M, NPQ, and q_P. The F_V/F_M was affected by the colony structure, and shaded surfaces were in a better physiological state than the exposed ones (Fig. 4B). As expected, the NPQ was higher and q_P was lower under high light conditions. The absolute values of F_V''/F_M'' were significantly affected by the colony structure. However, when the normalization to initial values of F_V/F_M was considered, the structure effects were not confirmed (Tab. 1).

Contrary to steady-state conditions, the rate of response of the photochemical light energy utilization (Φ_{PSII} and q_P; Fig. 5A,C) was influenced by colony structure only. The response to light was much faster and rapidly increased in the shaded surface of the colony. The NPQ was influenced by the light conditions only, and the response was faster under high light conditions (Tab. 2, Fig. 5B).

Discussion

The method of vertical stacking of individual light microscopy images proved to be suitable for determination of the 3D structure of *Nostoc* sp. colonies under the conditions at the field polar station. Although this approach is very time consuming and requires precise manual microscope control, its main advantage is minimum duration of sample transport and processing, as the prolonged sample storage and further transport to a specialized microscopy laboratory may affect the sample structure, or inadvertently change its orientation.

Using this approach, the 3D internal structure of the *Nostoc* sp. colony was visualized. The maximum filament density, and hence number of cells, was found in the central part of the colony. Similar cell and filament distribution was described in *Nostoc* sphaeroides colonies [20]. Reduced numbers of viable cell at the consortium surface is a common protection strategy [38,39]. The superficial extracellular matrix layers may provide protection against desiccation and freezing [3,24,40–45]. The screening pigments localized at the surface protect the cells against excessive radiation [46–48].

The vertical profile of the colony revealed two peaks of maximum cell density. This may reflect differences in morphology of experimental *Nostoc* sp. colonies and *N. sphaeroides* colonies [20]. Contrary to spherical *N. sphaeroides* [20], the experimental

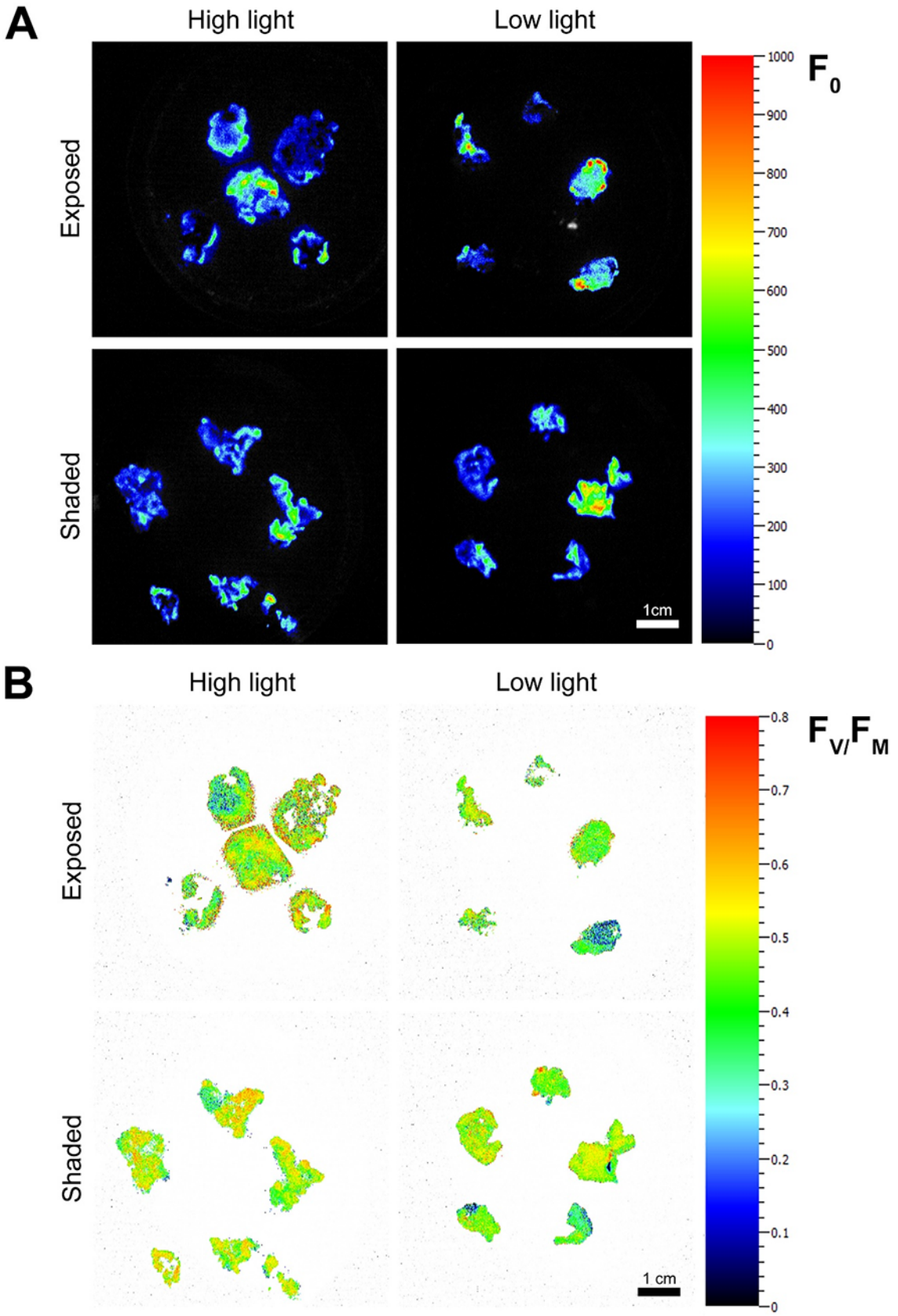

Fig. 4 The heterogeneity (**A**) of F_0, used as a chlorophyll content proxy, and (**B**) of the F_V/F_M as a proxy of the physiological status of the colonies.

Tab. 1 Fluorescence parameters of the exposed and shaded surfaces of the *Nostoc* sp. colonies (mean ±*SD*, $n = 5$ in each group) under high- and low-light conditions. The Φ_{PSII}, NPQ, and q_P shown indicate the steady-state at the end of the actinic light period.

	High light conditions		Low light conditions		
	Exposed	Shaded	Exposed	Shaded	Effects
F_0	193 ±49 [a]	233 ±43 [a]	271 ±82 [a]	242 ±84 [a]	
F_V/F_M	0.464 ±0.051 [ab]	0.520 ±0.020 [a]	0.412 ±0.063 [b]	0.450 ±0.051 [ab]	L/S
F_V''/F_M''	0.432 ±0.033 [ab]	0.482 ±0.023 [a]	0.404 ±0.032 [b]	0.442 ±0.047 [ab]	S
% F_V/F_M	93.4 ±3.6* [a]	92.7 ±3.9* [a]	99.0 ±7.2* [a]	98.2 ±2.7* [a]	
Φ_{PSII}	0.246 ±0.034 [a]	0.226 ±0.009 [a]	0.248 ±0.033 [a]	0.272 ±0.047 [a]	
NPQ	0.140 ±0.047 [a]	0.162 ±0.024 [a]	0.112 ±0.041 [a]	0.100 ±0.028 [a]	L
q_P	0.568 ±0.066 [ab]	0.470 ±0.020 [a]	0.642 ±0.073 [b]	0.636 ±0.053 [b]	L

The superscript indicates homologous groups recognized by Tukey HSD test at $p = 0.05$. "Effects" column shows significance of effects of structure (S) and light (L) on the fluorescence parameters. L/S indicates that only L (light) and only structure (S) effects were significant, but not their combination. Statistical significance expressed as p values: $p < 0.01$ and $p < 0.05$ (denoted by an asterisk).

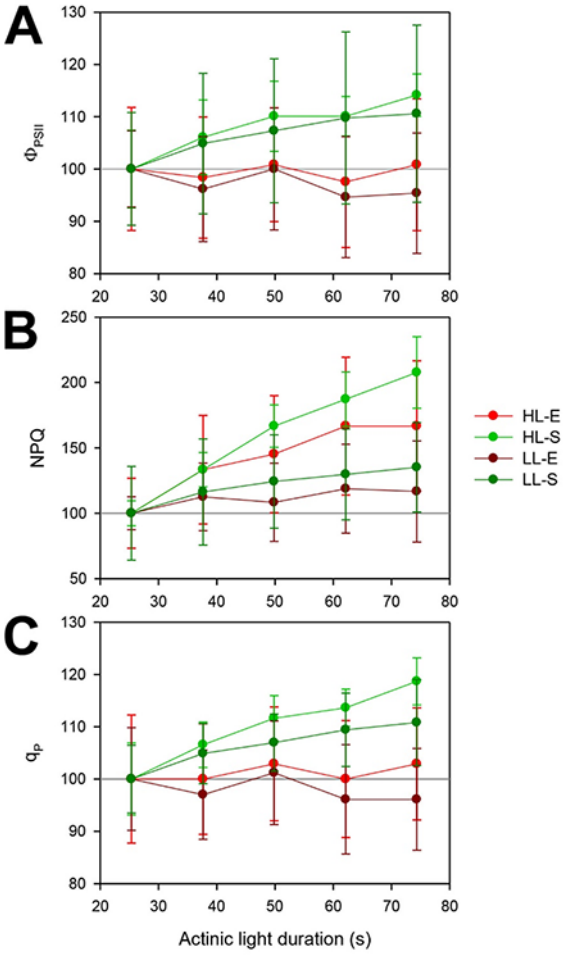

Fig. 5 The response of the fluorescence parameters (**A**) effective quantum yield, Φ_{PSII}, (**B**) nonphotochemical quenching, NPQ, and (**C**) photochemical quenching, q_P (mean ±*SD*, $n = 5$ in each group) to prolonged exposition to actinic light. The data were normalized to the values corresponding to the first saturation pulse during the actinic light period. Abbreviations: HL-E – high light, exposed surface; HL-S – high light, shaded surface; LL-E – low light, exposed surface; LL-S – low light, shaded surface.

Nostoc sp. colonies were flat and several hundred µm thick. Colonies of different morphology may be found in different habitats, which either reflects adaptation to environmental conditions [49], or represents different *Nostoc* species [50,51]. The visualization of the mucilaginous matrix revealed microscopic lobes or subcolonies, and their overlapping may result in the observed two peaks. These microscopic lobes or subcolonies have been previously documented in some *Nostoc* species [51].

Fluorescence imaging revealed heterogeneity of photosynthetic activity, which was highest at the edges and lowest in the colony centers. The higher photosynthetic activity could cover increased energy requirements, since the maximum growth was observed at edges of the colonies, probably due to better access to nutrients, mainly nitrogen and phosphorus [52,53].

In order to avoid the effects of colony size on photosynthesis [9,10], colonies of similar size were collected. Light was found to be the main driving factor of photosynthesis in *Nostoc* sp. colonies. The slightly higher F_V/F_M indicated a better physiological state of the shaded surface, apparently due to shielding by the filaments above. The lower F_V/F_M at exposed surfaces probably cannot be explained by partial submersion of the colony in seepage water or by desiccation due to wind, since the colonies must lose at least 50% of their fully hydrated weight before a decrease in photosynthetic activity is observed [54,55].

Since up to ca. 90% of incoming radiation could be absorbed in a ca. 100 µm layer of *Nostoc* sp. cells [56] depending on the colony structure, there should be distinct light conditions on the exposed and shaded surfaces. The different light conditions should lead to different patterns of light energy utilization that could be detected easily using the variable chlorophyll approach. In general, the effective quantum yield should be low, and NPQ should be higher on the exposed side, while on the shaded surface, the trend should be the opposite. Surprisingly, the light energy utilization in experimental colonies, expressed

Tab. 2 The rate of change of Φ_{PSII}, NPQ, and q_P (mean ±*SD*, $n = 5$ in each group; ×1,000 s^{-1}) in *Nostoc* sp. colonies under high- and low-light conditions.

	High light conditions		Low light conditions		
	Exposed	Shaded	Exposed	Shaded	Effects
Φ_{PSII}	0.016 ±0.227 [ab]	0.522 ±0.210 [a]	−0.229 ±0.244 [b]	0.523 ±0.428 [a]	S**
NPQ	1.143 ±0.524 [ab]	1.714 ±0.403 [a]	0.310 ±0.555 [b]	0.506 ±0.352 [b]	L**
q_P	0.261 ±0.578 [ab]	1.437 ±0.349 [a]	−0.474 ±0.806 [b]	1.225 ±0.993 [a]	S*

The superscript indicates homologous groups recognized by Tukey HSD test at $p = 0.05$. "Effects" column shows significance of effects of structure (S) and light (L) on the fluorescence parameters. L/S indicates that only L (light) and only structure (S) effects were significant. Statistical significance expressed as p value: * $p < 0.01$; ** $p < 0.001$.

as the effective quantum yield, and only slightly elevated NPQ and reduced q_P under high light conditions indicate increased nonphotochemical dissipation of light energy. Since *Nostoc* sp. colonies were found to be resistant to photoinhibition [56] and to express good photoacclimation to incoming light [58], the Arctic colonies should also be adapted to a broad range of light conditions. Despite completely different light conditions at exposed and shaded surfaces, photosynthesis in *Nostoc* sp. remains stable due to effective photoacclimation. It is also possible that the mucilaginous sheaths and colonial mucilage may serve as fiber optics to deliver photons to individual filaments, thus creating stable light conditions inside the colony. This would explain why no differences in photosynthetic activity were observed on shaded and exposed surfaces of *Nostoc* sp. colonies, as this would mean that the fluorescence signal would be integrated throughout the colonies. This hypothesis on colonial mucilage serving as a fiber optics must be tested experimentally.

Since a better physiological state of the Arctic *Nostoc* sp. colonies was found under high-light conditions, *Nostoc* sp. colonies seem to be well adapted for survival in open areas like seepages or wet tundra [31]. Detailed investigation of photosynthesis in Arctic *Nostoc* sp. colonies should be performed, including measurements of photosynthesis-irradiance (PE) curves under different light regimes, to determine the photoacclimation range of polar *Nostoc* sp. colonies in detail.

Acknowledgments

I am thankful to Josef Elster, University of South Bohemia, for critical review of the manuscript, and to Kamil Láska, Masaryk University in Brno, for global radiation data on dates of measurements, from which approximate PAR data were calculated.

References

1. Broady PA. Diversity, distribution and dispersal of Antarctic algae. Biodivers Conserv. 1996;5:1307–1335. https://doi.org/10.1007/BF00051981
2. Elster J. Ecological classification of terrestrial algal communities in polar environments. In: Beyer L, Bötler M, editors. Geoecology of Antarctic ice-free coastal landscapes. Springer; 2002. p. 303–326. (Ecological Studies; vol 154). https://doi.org/10.1007/978-3-642-56318-8_17
3. Elster J, Benson EE. Life in the polar terrestrial environment with a focus on algae and cyanobacteria. In: Fuller BJ, Lane N, Benson EE, editors. Life in the frozen state. Boca Raton, FL: CRC Press; 2004. p. 111–150. https://doi.org/10.1201/9780203647073.ch3
4. Vincent WF. Cyanobacterial dominance in the Polar regions. In: Whitton BA, Potts M, editors. The ecology of cyanobacteria. Dordrecht: Kluwer Academic Publishers; 2000. p. 321–340. https://doi.org/10.1007/0-306-46855-7_12
5. Zakhia F, Jungblut AD, Taton A, Vincent WF, Wilmotte A. Cyanobacteria

in cold ecosystems. In: Margesin R, Schinner F, Marx JC, Gerday C, editors. Psychrophiles: from biodiversity to biotechnology. Berlin: Springer; 2008. p. 121–135. https://doi.org/10.1007/978-3-540-74335-4_8

6. Jungblut AD, Vincent WF. Cyanobacteria in the polar and alpine ecosystems. In: Margesin R, editor. Psychrophiles: from biodiversity to biotechnology. Cham: Springer; 2017. p. 181–206. https://doi.org/10.1007/978-3-319-57057-0_9
7. Morgan-Kiss RM, Priscu JC, Pocock T, Gudynaite-Savitch L, Huner NPA. Adaptation and acclimation of photosynthetic microorganisms to permanently cold environments. Microbiol Mol Biol Rev. 2006;70(1):222–252. https://doi.org/10.1128/MMBR.70.1.222-252.2006
8. Schulze ED, Beck E, Müller-Hohenstein K. Plant ecology. Berlin: Springer; 2005.
9. Gao K, Ai H. Relationship of growth and photosynthesis with colony size in an edible cyanobacterium, Ge-Xian-Mi *Nostoc* (Cyanophyceae). J Phycol. 2004;40:523–526. https://doi.org/10.1111/j.1529-8817.2004.03155.x
10. Li Y, Gao K. Photosynthetic physiology and growth as a function of colony size in the cyanobacterium *Nostoc sphaeroides*. Eur J Phycol. 2004;39:9–15. https://doi.org/10.1080/0967026032000157147
11. Paerl HW, Pinckney JL, Steppe TF. Cyanobacterial-bacterial mat consortia: examining the functional unit of microbial survival and growth in extreme environments. Environ Microbiol. 2000;2(1):11–26. https://doi.org/10.1046/j.1462-2920.2000.00071.x
12. Belnap J, Lange OL. Structure and functioning of biological soil crusts: a synthesis. In: Belnap J, Lange OL, editors. Biological soil crusts: structure, function, and management. Berlin: Springer; 2001. p. 471–479. https://doi.org/10.1007/978-3-642-56475-8_33
13. Pushkareva E, Johansen JR, Elster J. A review of the ecology, ecophysiology and biodiversity of microalgae in Arctic soil crusts. Polar Biol. 2016;39(12):2227–2240. https://doi.org/10.1007/s00300-016-1902-5
14. Schneider T, Schmid E, de Castro JV, Cardinale M, Eberl L, Grube M, et al. Structure and function of the symbiosis partners of the lung lichen (*Lobaria pulmonaria* L. Hoffm.) analyzed by metaproteomics. Proteomics. 2011;11(13):2752–2756. https://doi.org/10.1002/pmic.201000679
15. Tashyreva D, Elster J. Production of dormant stages and stress resistance of polar cyanobacteria. In: Hanslmeier A, Kempe S, Seckbach J, editors. Life on Earth and other planetary bodies. Dordrecht: Springer; 2012. p. 367–386. https://doi.org/10.1007/978-94-007-4966-5_21
16. Aguilera A, Souza-Egipsy V, Gomez F, Amils R. Development and structure of eukaryotic biofilms in an extreme acidic environment, Rio Tinto (SW, Spain). Microb Ecol. 2007;53(2):294–305. https://doi.org/10.1007/s00248-006-9092-2
17. Flemming HC, Wingender J. The biofilm matrix. Nat Rev Microbiol. 2010;8(9):623–633. https://doi.org/10.1038/nrmicro2415
18. Kvíderová J. Biofilm. In: Amils R, Gargaud M, Cernicharo Quintanilla J, Cleaves HJ, Irvine WM, Pinti D, et al., editors. Encyclopedia of astrobiology. Berlin: Springer; 2015. p. 1–3. https://doi.org/10.1007/978-3-642-27833-4_170-3
19. Tamaru Y, Takani Y, Yoshida T, Sakamoto T. Crucial role of extracellular polysaccharides in desiccation and freezing tolerance in the terrestrial cyanobacterium *Nostoc commune*. Appl Environ Microb. 2005;71(11):7327–7333. https://doi.org/10.1128/aem.71.11.7327-7333.2005
20. Deng Z, Hu Q, Lu F, Liu G, Hu Z. Colony development and physiological characterization of the edible blue-green alga, *Nostoc sphaeroides* (Nostocaceae, Cyanophyta). Prog Nat Sci. 2008;18(12):1475–1483. https://doi.org/https://doi.org/10.1016/j.pnsc.2008.03.031
21. Armstrong R, Bradwell T. Growth of crustose lichens: a review. Geografiska Annaler: Series A, Physical Geography. 2010;92(1):3–17. https://doi.org/10.1111/j.1468-0459.2010.00374.x
22. Wharton RA, Parker BC, Simmons GM. Distribution, species composition and morphology of algal mats in Antarctic dry valley lakes. Phycologia. 1983;22(4):355–365. https://doi.org/10.2216/i0031-8884-22-4-355.1
23. MacIntyre HL, Geider RJ, Miller DC. Microphytobenthos: the ecological role of the "secret garden" of unvegetated, shallow-water marine habitats. I. Distribution, abundance and primary production. Estuaries. 1996;19(2):186–201. https://doi.org/10.2307/1352224

24. de los Ríos A, Ascaso C, Wierzchos J, Fernández-Valiente E, Quesada A. Microstructural characterization of cyanobacterial mats from the McMurdo Ice Shelf, Antarctica. Appl Environ Microb. 2004;70(1):569–580. https://doi.org/10.1128/aem.70.1.569-580.2004
25. Komárek O, Komárek J. Diversity and ecology of cyanobacterial microflora of Antarctic seepage habitats: comparison of King George Island, Shetland Islands, and James Ross Island, NW Weddell Sea, Antarctica. In: Seckbach J, Oren A, editors. Microbial mats: modern and ancient microorganisms in stratified systems. Dordrecht: Springer; 2010. p. 515–539. https://doi.org/10.1007/978-90-481-3799-2_27
26. Taton A, Grubisic S, Brambilla E, de Wit R, Wilmotte A. Cyanobacterial diversity in natural and artificial microbial mats of Lake Fryxell (McMurdo Dry Valleys, Antarctica): a morphological and molecular approach. Appl Environ Microb. 2003;69(9):5157–5169. https://doi.org/10.1128/aem.69.9.5157-5169.2003
27. Revsbech NP, Jorgensen BB, Blackburn TH, Cohen Y. Microelectrode studies of the photosynthesis and O_2, H_2S, and pH profiles of a microbial mat. Limnol Oceanogr. 1983;28(6):1062–1074. https://doi.org/10.4319/lo.1983.28.6.1062
28. Glud RN, Kühl M, Kohls O, Ramsing NB. Heterogeneity of oxygen production and consumption in a photosynthetic microbial mat as studied by planar optodes. J Phycol. 1999;35(2):270–279. https://doi.org/10.1046/j.1529-8817.1999.3520270.x
29. Vopel K, Hawes I. Photosynthetic performance of benthic microbial mats in Lake Hoare, Antarctica. Limnol Oceanogr. 2006;51(4):1801–1812. https://doi.org/10.4319/lo.2006.51.4.1801
30. Secker NH., Chua JPS, Laurie RE, McNoe L, Guy PL, Orlovich DA, et al. Characterization of the cyanobacteria and associated bacterial community from an ephemeral wetland in New Zealand. J Phycol. 2016;52(5):761–773. https://doi.org/10.1111/jpy.12434
31. Komárek J, Kováčik L, Elster J, Komárek O. Cyanobacterial diversity of Petuniabukta, Billefjorden, central Spitzbergen. Pol Polar Res. 2012;33(4):347–368. https://doi.org/10.2478/v10183-012-0024-1
32. Nedbal L, Soukupová J, Kaftan D, Whitmarsh J, Trtílek M. Kinetic imaging of chlorophyll fluorescence using modulated light. Photosynth Res. 2000;66:3–12. https://doi.org/10.1023/A:1010729821876
33. Nedbal L, Whitmarsh J. Chlorophyll fluorescence imaging of leaves and fruits. In: Papageorgiou GC, Govindjee, editors. Chlorophyll *a* fluorescence. A signature of photosynthesis. Dordrecht: Springer; 2004. p. 389–407. (Advances in Photosynthesis and Respiration; vol 19). https://doi.org/10.1007/978-1-4020-3218-9_14
34. Schneider CA, Rasband WS, Eliceiri KW. NIH Image to ImageJ: 25 years of image analysis. Nat Method. 2012;9:671. https://doi.org/10.1038/nmeth.2089
35. Roháček K, Soukupová J, Barták M. Chlorophyll fluorescence: a wonderful tool to study plant physiology and plant stress. In: Schoefs B, editor. Plant cell compartments-selected topics. Kerala: Research Signpost; 2008. p. 41–104.
36. Oxborough K, Baker NR. Resolving chlorophyll *a* fluorescence images of photosynthetic efficiency into photochemical and non-photochemical components – calculation of qP and Fv′/Fm′; without measuring Fo′. Photosynth Res. 1997;54(2):135–142. https://doi.org/10.1023/A:1005936823310
37. Statsoft. Statistica, version 13. 2015 [cited 2018 Dec 29]. Available from: http://www.statsoft.com/Products/STATISTICA-Features
38. Vincent WF, Castenholz RW, Downes MT, Howard-Williams C. Antarctic cyanobacteria: light, nutrients, and photosynthesis in the microbial mat environment. J Phycol. 1993;29(6):745–755. https://doi.org/10.1111/j.0022-3646.1993.00745.x
39. Vincent WF, Downes MT, Castenholz RW, Howard-Williams C. Community structure and pigment organisation of cyanobacteria-dominated microbial mats in Antarctica. Eur J Phycol. 1993;28(4):213–221. https://doi.org/10.1080/09670269300650321
40. Hawes I, Howard-Williams C, Vincent W. Desiccation and recovery of antarctic cyanobacterial mats. Polar Biol. 1992;12(6):587–594. https://doi.org/10.1007/BF00236981
41. Potts M. Desiccation tolerance of prokaryotes. Microbiol Mol Biol Rev. 1994;58(4):755–805.
42. Potts M. Mechanisms of desiccation tolerance in cyanobacteria. Eur J Phycol. 1999;34:319–328. https://doi.org/10.1080/09670269910001736382
43. Tashyreva D, Elster J. Annual cycles of two cyanobacterial mat communities in

hydro-terrestrial habitats of the high Arctic. Microb Ecol. 2016;71(4):887–900. https://doi.org/10.1007/s00248-016-0732-x

44. Makhalanyane TP, Valverde A, Velázquez D, Gunnigle E, van Goethem MW, Quesada A, et al. Ecology and biogeochemistry of cyanobacteria in soils, permafrost, aquatic and cryptic polar habitats. Biodivers Conserv. 2015;24(4):819–840. https://doi.org/10.1007/s10531-015-0902-z
45. Deming JW, Young JN. The role of exopolysaccharides in microbial adaptation to cold habitats. In: Margesin R, editor. Psychrophiles: from biodiversity to biotechnology. Cham: Springer; 2017. p. 259–284. https://doi.org/10.1007/978-3-319-57057-0_12
46. Cockell CS, Knowland J. Ultraviolet radiation screening compounds. Biol Rev. 1999;79:311–345. https://doi.org/10.1017/S0006323199005356
47. Garcia-Pichel F, Castenholz RW. Occurrence of UV-absorbing, mycosporine-like compounds among cyanobacterial isolates and an estimate of their screening capacity. Appl Environ Microb. 1993;59(1):163–169.
48. Sinha RP, Klisch M, Gröniger A, Häder DP. Ultraviolet-absorbing/screening substances in cyanobacteria, phytoplankton and macroalgae. J Photochem Photobiol B. 1998;47(2–3):83–94. https://doi.org/https://doi.org/10.1016/S1011-1344(98)00198-5
49. Dodds WK. Photosynthesis of two morphologies of *Nostoc parmelioides* (Cyanobacteria) as related to current velocities and diffusion patterns. J Phycol. 1989;25(2):258–262. https://doi.org/10.1111/j.1529-8817.1989.tb00121.x
50. Komárek J. Süßwasserflora von Mitteleuropa 19/3. Cyanoprokaryota. 3. Teil: Heterocytous genera. Heildelberg: Springer; 2013. https://doi.org/10.1007/978-3-8274-2737-3
51. Hrouzek P, Ventura S, Lukešová A, Mugnai MA, Turicchia S, Komárek J. Diversity of soil *Nostoc* strains: phylogenetic and phenotypic variability. Algol Stud. 2005;117(1):251–264. https://doi.org/10.1127/1864-1318/2005/0117-0251
52. Lukavský J. Controlled cultivation of algae on agar plates. Algol Stud. 1974;10:90–104.
53. Lukavský J. Analysis of growth rate of algae by cultivation on solid media. Algol Stud. 1975;14:105–136.
54. Kvíderová J, Elster J, Šimek M. In situ response of *Nostoc commune* s. l. colonies to desiccation in central Svalbard, Norwegian high Arctic. Fottea. 2011;11(1):87–97. https://doi.org/10.5507/fot.2011.009
55. Gao K, Qiu B, Xia J, Yu A, Li Y. Effect of wind speed on loss of water from *Nostoc flagelliforme* colonies. J Appl Phycol. 1998;10(1):55–58. https://doi.org/10.1023/A:1008020914486
56. Dodds WK, Gudder DA, Mollenhauer D. The ecology of *Nostoc*. J Phycol. 1995;31(1):2–18. https://doi.org/10.1111/j.0022-3646.1995.00002.x
57. Fukuda S, Yamakawa R, Hirai M, Kashino Y, Koike H, Satoh K. Mechanisms to avoid photoinhibition in a desiccation-tolerant cyanobacterium, *Nostoc commune*. Plant Cell Physiol. 2008;49(3):488–492. https://doi.org/10.1093/pcp/pcn018
58. Poza-Carrión C, Fernández-Valiente E, Piñas FF, Leganés F. Acclimation of photosynthetic pigments and photosynthesis of the cyanobacterium *Nostoc* sp. strain UAM206 to combined fluctuations of irradiance, pH, and inorganic carbon availability. J Plant Physiol. 2001;158(11):1455–1461. https://doi.org/10.1078/0176-1617-00555